THE JOURNAL OF PHYSICAL CHEMISTRY B

Article

pubs.acs.org/JPCB

# Relationship between Structural Relaxation, Shear Viscosity, and Ionic Conduction of $LiPF_6$/Propylene Carbonate Solutions

Tsuyoshi Yamaguchi,[*,†] Takuya Yonezawa,[†] Koji Yoshida,[‡] Toshio Yamaguchi,[‡] Michihiro Nagao,[§,∥] Antonio Faraone,[§] and Shiro Seki[⊥]

[†]Department of Molecular Design and Engineering, Graduate School of Engineering, Nagoya University, Furo-cho, Chikusa, Nagoya, Aichi 464-8603, Japan

[‡]Department of Chemistry, Faculty of Science, Fukuoka University, Nanakuma, Jonan, Fukuoka 814-0180, Japan

[§]NIST Center for Neutron Research, National Institute of Standards and Technology, Gaithersburg, Maryland 20899-6102, United States

[∥]Center for Exploration of Energy and Matter, Indiana University, Bloomington, Indiana 47408-1398, United States

[⊥]Materials Science Research Laboratory, Central Research Institute of Electric Power Industry (CRIEPI), 2-11-1, Iwado-kita, Komae, Tokyo 201-8511, Japan

Supporting Information

**ABSTRACT:** The structure and dynamics of the solutions of $LiPF_6$ in propylene carbonate over a concentration range of 0−3 mol/kg are studied with neutron spin echo spectroscopy, alternating-current (AC) conductometry, and shear impedance spectroscopy. The neutron diffraction shows a prepeak at ≈10 $nm^{-1}$ in addition to the main peak at ≈14 $nm^{-1}$ when the concentration of the salt is no less than 2 mol/kg. Compared with the frequency-dependent shear viscosity and AC conductivity, the relaxation of the shear stress agrees with that expected from the structural relaxation of the main peak. On the other hand, the relaxation of the conductivity is slower than the shear relaxation at all the concentrations, and the former approximately matches with the relaxation of the prepeak at the highest concentration, 3 mol/kg, which is several times slower than that of the main peak. The possible contribution of the prepeak structure to the ionic conduction is discussed.

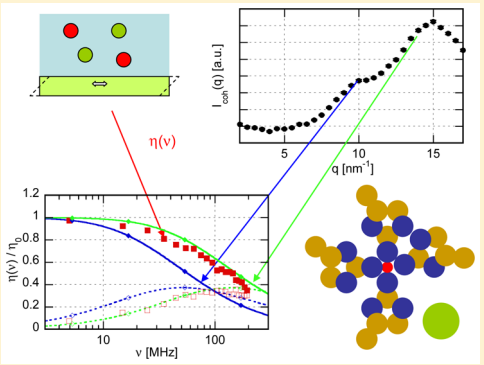


## 1. INTRODUCTION

The attention to organic electrolytes, including ionic liquids and concentrated solutions of salts in organic solvents, has been growing for the past decades owing to their industrial and scientific importance.[1,2] Although the studies on organic electrolytes in earlier days have been performed as basic science, the applications of organic electrolytes are growing because of the wider electrochemical window compared with aqueous electrolytes.

In addition to the trivial merit of the high carrier density, the increase in the salt concentration of organic electrolytes sometimes leads to the improvement of the electrochemical stability.[3,4] On the other hand, the viscosity of the organic electrolytes increases rapidly with increasing the concentration of the salt, which usually accompanies a decrease in the ionic mobility.[5−7] The increase in the shear viscosity of organic electrolytes with concentration is much larger than that of aqueous electrolytes, and its microscopic origin is not clarified yet. The rapid increase in viscosity may relate to the slow dynamics of supercooled liquids, which is another important issue in material science. Therefore, it is of both academic and industrial demands to understand the molecular mechanisms that determine the shear viscosity and the ionic conductivity of concentrated organic electrolyte solutions.

The transport coefficients, such as the shear viscosity and the ionic conductivity, are dynamic properties determined by the molecular dynamics of the solution. Kubo−Green theory states that they are given by the time integral of the corresponding time correlation functions.[8,9] For instance, the shear viscosity and ionic conductivity are related to the relaxation of the shear stress and of the ionic current, respectively. Therefore, the microscopic understanding of the transport properties is equivalent to the identification of the microscopic liquid dynamics coupled to the physical quantities that determine the transport coefficient.

Mode-coupling theory (MCT) is a first-principles theory based on statistical mechanics that describes the transport properties of liquids in terms of the structural relaxation.[8,10] The intermediate scattering function, which is the time correlation function of the density fluctuation at a finite wavevector, plays an important role in the MCT description of

**Received:** September 6, 2015
**Revised:** December 3, 2015
**Published:** December 3, 2015





DOI: 10.1021/acs.jpcb.5b08701
J. Phys. Chem. B 2015, 119, 15675−15682

the transport properties. The time correlation functions related to the transport properties are given by the superposition of the bilinear form of the intermediate scattering function. Therefore, MCT describes the transport coefficient as the sum of the contributions of the intermediate scattering functions at different wavevectors. Since the intermediate scattering function represents the structural relaxation at a wavevector, MCT connects the structural relaxation to the transport coefficients.

The time correlation functions related to the transport properties can be probed through the measurement of the frequency dependence of the transport coefficients. On the other hand, the intermediate scattering function can be determined with neutron or X-ray quasi-elastic scattering. MCT relates these relaxation functions to clarify the microscopic mechanisms on the transport properties. We have applied this methodology to the shear viscosity and the ionic conductivity of some ionic liquids.[11]

The static structure factor of simple liquids in general possesses a large peak at the wavevector corresponding to the reciprocal contact distance between molecules, which is hereafter called the "main peak". The main peak describes the packing structure of molecules in dense liquids. The relaxation time of the intermediate scattering function as a function of wavevector shows a maximum at the main peak, which is called "de Gennes narrowing".[10] Because of the large fluctuation and the slow dynamics of the main peak, the macroscopic transport properties of molecular liquids is usually governed by the structural relaxation at the main peak.[10]

There were many experimental studies on the intermediate scattering functions of supercooled liquids at the main peak, in which the temperature dependence of the relaxation time was compared with that of the shear viscosity in the zero-frequency limit.[12−16] The temperature dependence of both quantities agrees with each other in many cases, in harmony with the idea of the dominant role of the dynamics at the main peak in determining the shear viscosity. However, the agreement of the temperature dependence alone cannot be the definite proof, since the temperature dependence of so many dynamic quantities of liquids follows that of the shear viscosity, and we believe that the comparison of the shear relaxation time with the relaxation time of the intermediate scattering function is indispensable.

The structure factors of some liquids show a small peak at wavevectors lower than the main peak, which is called "prepeak". Since the lower wavevector corresponds to larger length scale in the real space, the prepeak indicates the presence of an intermediate range structure. The famous example of the prepeak is that of molten silica, which originates from the tetrahedral network structure.[17] Another example is those of hydrogen-bonding liquids[18−20] and ionic liquids with long alkyl chain,[21−24] which are ascribed to the mesoscopic segregation between the polar and the nonpolar domains.

The prepeak structure of ionic liquids has attracted the interest of many researchers, and the relationship between the intermediate range structure and shear viscosity has also been discussed.[25] We compared the intermediate scattering function with the frequency-dependent transport coefficient for ionic liquids with long alkyl chains[11,26] and found that the relaxations of the shear stress and the ionic current are comparable to that of the main peak when the viscosity is low. With increasing the viscosity, the former two become slower than the latter, and the magnitude of the decoupling is larger for viscosity than for ionic conductivity.

The same methodology is applied in this work to the solution of lithium hexafluorophosphate in propylene carbonate ($LiPF_6$/PC), which is a representative model electrolyte for lithium ion secondary battery. Applying the neutron spin echo (NSE) spectroscopy, we first demonstrate that the prepeak structure is present in concentrated $LiPF_6$/PC solutions and that the relaxation of the prepeak is slower than that of the main peak. The frequency dependence of the shear viscosity and the electric conductivity were then measured at the same conditions, and they were compared with the intermediate scattering functions at the two peaks to clarify the role of these structures in determining the shear viscosity and the ionic conductivity.

## 2. THEORETICAL BACKGROUND

According to the Kubo−Green theory, the frequency-dependent shear viscosity, $\eta(\nu)$, is described in terms of the Fourier transform of the time correlation function of the shear stress tensor, $\Pi_{xz}(t)$, as[8,9]

$$\eta(\nu) = \frac{1}{k_B TV}\int_0^\infty \mathrm{d}t\ \mathrm{e}^{-2\pi i\nu t}\langle \Pi_{xz}(0)\Pi_{xz}(t)\rangle \tag{1}$$

where $k_B$, $T$, and $V$ stand for the Boltzmann constant, the absolute temperature, and the volume of the system, respectively. The frequency-dependent shear viscosity is equivalent to the memory function of the transverse momentum density in the frequency domain. The steady-state shear viscosity, $\eta_0$, is the zero-frequency value of $\eta(\nu)$.

Similarly, the AC electric conductivity, $\sigma(\nu)$, is related to the time correlation function of the electric current, $\mathbf{j}_{el}(t)$, as

$$\sigma(\nu) = \frac{1}{k_B TV}\int_0^\infty \mathrm{d}t\ \mathrm{e}^{-2\pi i\nu t}\langle j_{el,z}(0)j_{el,z}(t)\rangle \tag{2}$$

In the case of the direct-current (DC) conductivity, $\sigma_0 \equiv \sigma(0)$, the total electric current in eq 2 can be replaced with its ionic contribution, $\mathbf{j}_I(t)$, and it is only the translational motion of ions that contributes to the DC conductivity. However, the reorientational motion of polar solvents induces the time-dependent electric current, which is also included in $\mathbf{j}_{el}(t)$. It is thus impossible in principle to separate the contributions of the ions and polar solvents to the AC conductivity solely on experimental basis. To be noted here is that although the reorientational motion of ions may also contribute to the AC conductivity in general, it can be neglected in the present case owing to the high symmetry of the molecular shapes of ions used in this work, $Li^+$ and $PF_6^-$.

The AC ionic conductivity, $\sigma_I(\nu)$, is defined here in the analogy of eq 2 as

$$\sigma_I(\nu) = \frac{1}{k_B TV}\int_0^\infty \mathrm{d}t\ \mathrm{e}^{-2\pi i\nu t}\langle j_{I,z}(0)j_{I,z}(t)\rangle \tag{3}$$

Its zero-frequency value, $\sigma_I(0)$, equals to the DC conductivity, $\sigma_0$. Based on the generalized Langevin theory, $\sigma_I(\nu)$ is reciprocally proportional to the memory function for the ionic current in the frequency-domain, $\xi(\nu)$, in the diffusive limit as

$$\sigma_I(\nu) \propto 1/\xi(\nu) \tag{4}$$



DOI: 10.1021/acs.jpcb.5b08701
J. Phys. Chem. B 2015, 119, 15675−15682

where the physical meaning of $\xi(\nu)$ is the friction coefficient on the ionic current. The frequency-dependent Walden rule, $\sigma_I(\nu)\eta(\nu)$ = constant, holds when $\xi(\nu)$ is proportional to $\eta(\nu)$.

MCT describes the memory function in the time domain, $K(t)$, as a linear combination of bilinear form of the density−density correlation functions at finite wavevectors. In the case of MCT based on the interaction-site description, $K(t)$ is generally given by[27]

$$K(t) \propto \int \mathrm{d}^3q \sum_{\alpha\alpha'\gamma\gamma'} V_{\alpha\alpha'}(q)F_{\alpha\gamma}(q, t)F_{\alpha'\gamma'}(q, t)V_{\gamma\gamma'}(q) \tag{5}$$

where the Greek letters are the indices for interaction sites, $F_{\alpha\gamma}(q,t)$ denotes the site−site intermediate scattering function, and $V_{\alpha\gamma}(q)$ does the vertex function that describes the coupling strength between the random force and the density modes.

The information on the site−site intermediate scattering function can be probed by the quasi-elastic scattering experiment. The intermediate scattering function determined in the neutron experiment, $I_n(q,t)$, is related to $F_{\alpha\gamma}(q,t)$ as

$$I_n(q, t) = \sum_{\alpha\gamma} b_\alpha b_\gamma F_{\alpha\gamma}(q, t) \tag{6}$$

where $b_\alpha$ stands for the neutron scattering length of the $\alpha$ atom.

Here we introduce two assumptions for the comparison between the structural relaxation and the frequency-dependent transport properties. The first one is that the time dependence of $F_{\alpha\gamma}(q,t)$ is given by that of $I_n(q,t)$ at the same wavevector irrespective of the sites, which means that the time scale of the structural relaxation is determined solely by the length scale of the structure. The second one is that the contribution of the structure around a particular wavevector, denoted as $q_m$, dominates the integral over $\mathbf{q}$ in eq 5. The latter approximation is known to hold approximately for simple dense liquids, and $q_m$ corresponds to the main peak of the static structure factor.[10]

Under the two assumptions above, eq 5 is transformed as

$$K(t) \propto I_n^2(q_m, t) \tag{7}$$

which is transformed into the frequency domain as

$$\tilde{K}(\nu) \equiv \int_0^\infty \mathrm{e}^{-2\pi i\nu t}K(t)\,\mathrm{d}t \propto \int_0^\infty \mathrm{e}^{-2\pi i\nu t}I_n^2(q_m, t)\,\mathrm{d}t \equiv S_2(q_m, \nu) \tag{8}$$

Based on eq 8, the functions $S_2(q,\nu)$ are calculated at various values of $q$ from the neutron intermediate scattering functions, e.g., at the main peak and at the prepeak, and they are compared with the memory functions related to the transport properties, $\eta(\nu)$ and $1/\sigma_I(\nu)$ for viscosity and ionic conductivity, respectively. The relaxation of the memory function will match with that of $S_2(q,\nu)$ when the structure at the wavevector $q$ determines the corresponding transport coefficient.

## 3. EXPERIMENTAL SECTION[46]

The sample solutions for NSE measurements were prepared by dissolving $LiPF_6$ (Lithium Battery grade, Kishida) into PC-$d_6$ (CDN Isotope). Both the solute and the solvent were used without purification. The molality of the samples was varied from 0 mol/kg (neat solvent) to 3 mol/kg with intervals of 1 mol/kg, where the molality of the deuterated solution $m$ mol/kg means that the molar ratio of $LiPF_6$ to PC-$d_6$ is equal to that of $m$ mol/kg $LiPF_6$/PC-$h_6$ solution. The concentration of 1 mol/kg corresponds to the molar ratio of $LiPF_6$: PC = 1:9.8. The sample preparation for neutron measurement was conducted under a He atmosphere with a moisture control.

The intermediate scattering functions from the samples were measured on NGA-NSE at the NIST Center for Neutron Research (NCNR).[28] The incident wavelength was selected using a neutron velocity selector to be 0.5 nm with a wavelength distribution of about 20%. In order to verify the structural features, we measured polarized diffraction for each sample at 1 $nm^{-1} \le q \le 17$ $nm^{-1}$. The diffraction patterns were also measured using the cold neutron spin-polarized triple-axis spectrometer (SPINS) at NCNR and with in-house small- and wide-angle X-ray apparatus in Fukuoka University; the results were consistent to each other within experimental error. The diffraction patterns showed the main peak centered at $q \approx 14$ $nm^{-1}$ and, in the $LiPF_6$ containing samples, the existence of a prepeak at $q \approx 10$ $nm^{-1}$, as will be described in the next section. The dynamics measurements were performed at these two $q$-values to investigate the dynamics at the prepeak and main peak, respectively. The relaxation behavior was measured in the time range from 5 ps to 10 ns. The sample temperature was controlled using a closed cycle refrigerator at 298 ± 1 K. The resolution function of the spectrometer was measured using the same sample below 10 K. The diffraction pattern at 10 K did not exhibit sharp Bragg peaks and resembles that of the liquid state, indicating that the sample solutions were supercooled to 10 K without crystallization. The normalized intermediate scattering functions $I(q,t)/I(q,0)$ were calculated using DAVE software[29] to correct for the instrumental resolution.

The solutions for the measurements of the frequency-dependent shear viscosity and electric conductivity were prepared under a $N_2$ atmosphere from $LiPF_6$ and PC-$h_6$, both of which were of Lithium Battery grade and purchased from Kishida Chemical. The solvent were dried with molecular sieves 3A (Kishida) prior to use.

The shear relaxation spectra were measured with the shear impedance spectroscopy, whose detailed descriptions were found in the literature.[7,30] Briefly, the shear impedance of the sample was determined from the change in the electric resonance of an AT-cut quartz crystal (QSX-301, Q-Sense). The fundamental frequency of the crystal was 5 MHz, and the shear impedances from 5 to 205 MHz were obtained by using the overtones up to the 41st one. The measurements of the electric resonance signal were performed with a bridge circuit and the vector network analyzer (ZVL3/03, Rhode & Schwartz), which was described in detail in our previous papers.[7,31] The frequency-dependent shear viscosity was calculated by dividing the shear impedance by the mass density. The temperature was controlled at 298.2 ± 0.2 K by flowing the thermostated water through the sample cell. The errors of the complex shear relaxation spectrum, $\eta(\nu)$, were estimated to be $|\delta\eta(\nu)/\eta(\nu)| < 0.1$ in the frequency region between 15 and 95 MHz and $|\delta\eta(\nu)/\eta(\nu)| < 0.2$ at other frequencies.

The AC electric conductivity was measured with the vector network analyzer (ZVL3/03, Rhode & Schwartz) through the electric impedance calculated from the complex reflectance, $S_{11}(\nu)$. The frequency range of the measurements was from 300 kHz to 3 GHz. The measurements at lower (300 kHz−200 MHz) and higher (200 MHz−3 GHz) frequency regions were performed separately, and the calibrations were also performed in different ways as are described in the next two paragraphs. The temperatures of the sample solutions were regulated at 298.2 ± 0.2 K in both measurements.



DOI: 10.1021/acs.jpcb.5b08701
J. Phys. Chem. B 2015, 119, 15675−15682

The homemade flat-type dielectric probe was used for the lower frequency AC conductometry, which was described in detail elsewhere.[32] The electric impedance of the probe including the sample solution was approximated as an equivalent circuit composed of the sample part, a capacitor, a resonator, and an inductor. The parameters for these hypothetical components were determined from the measurements of water and aqueous solutions of NaCl at various concentrations.[33] The DC conductivity was determined from the plateau value of $\sigma'(\nu)$ at 1−10 MHz. The measurements of the AC conductivity were performed twice, and the discrepancy of the two independent measurements was less than about ±10%.

The high-temperature dielectric probe (HP85070B, Hewlett-Packard) was used for the measurements of $\sigma(\nu)$ in a higher frequency region. The electric reflectance $S_{11}(\nu)$ was converted into the AC electric conductivity $\sigma(\nu)$ through the three-point calibration, whose reference fluids were air, methanol and 1 mol/dm$^3$ aqueous solution of NaCl.[28]

Density and steady-state viscosity were measured using a thermo-regulated Stabinger-type viscosity and density/specific gravity meter (Anton Paar, SVM3000G2), whose reproducibility is within 0.35%. The measurements were performed at 298.15 ± 0.02 K with an airtight stopper to avoid moisture and air contamination. The samples were thermally equilibrated for at least 15 min prior to the measurement.

## 4. RESULTS AND DISCUSSION

**4.1. Neutron Scattering.** Figure 1 shows the neutron diffraction patterns at various concentrations. The coherent scattering of the neat solvent possesses a single strong peak at 14 nm$^{-1}$ as is the case for most simple liquids. Hereafter we call this peak "main peak". The position of the main peak represents the contact distance between molecules in dense liquids. With increasing the salt concentration, the position of the main peak shifts to higher wavevector, while its width is broadened. Given that the sizes of the dissolved ions are smaller than that of the solvent, the high-$q$ shift of the main peak is understood in terms of the decrease in the molecular size on average with increased spatial inhomogeneity.

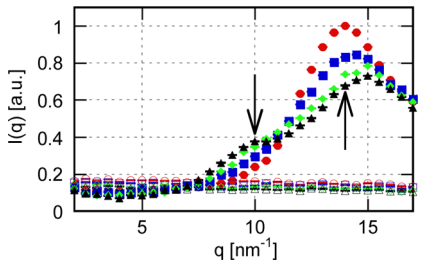


**Figure 1.** Neutron diffraction patterns at 298 K measured on the NSE spectrometer are plotted as a function of $q$. The coherent and incoherent parts are shown with filled and open symbols, respectively. The concentrations of the sample are 0 mol/kg (red circles), 1 mol/kg (blue squares), 2 mol/kg (green diamonds), and 3 mol/kg (black triangles), respectively. The two arrows indicate the wavevectors at which the intermediate scattering functions were measured.

In addition to the main peak, a small shoulder is found at 10 nm$^{-1}$, which is hereafter called the "prepeak". The height of the prepeak grows with increasing the salt concentration, while its position does not seem to change with the concentration. Since a lower wavevector corresponds to a larger scale structure, the prepeak indicates the presence of a structure larger than the molecular scale. The presence of the prepeak has been reported on various kinds of liquids, including molten silica,[12] hydrogen-bonding liquids,[13−15] and ionic liquids with long alkyl chains.[16−19] Very recently, Aguilera and co-workers demonstrated the existence of the prepeak of the concentrated solution of lithium bis(trifluoromethanesulfonyl)amide (TFSA) in tetraglyme,[34] which was also confirmed by MD simulation.[35]

Though we cannot give the definite assignment of an origin of the prepeak at present, we would like to present a tentative idea on the origin of the prepeak, which is in agreement with those of alcohols and ionic liquids. Recently, Seo and co-workers reported the *crystalline* structures of the concentrated mixture of lithium salts with ethylene carbonate (EC).[36] They demonstrated the structure in which the cations and anions are aligned alternately in line, and the solvents are coordinated with the cation from the side. The structure resembles the chain-like structure of 1-alcohols in that the chain of ions corresponds to the linear hydrogen-bond network while the solvent does to the alkyl chain. It is similar also to the domain structure of ionic liquid, regarding the methylene groups of EC as the nonpolar parts. Therefore, the prepeak of the $LiPF_6$/PC solutions can be explained as the chain-like structure in liquid solutions. Another candidate of the assignment is the charge alternation,[37] as is proposed by Aguilera and co-workers on LiTFSA−tetraglyme solution based on the correspondence between the peak position of the prepeak and the interionic separation of the solvent-separated ion pair.[30] Preliminary results of the X-ray scattering of the solutions of $LiPF_6$ in PC and butylene carbonate, whose alkyl chain is longer than that of PC, are presented in the Supporting Information. The prepeak is enhanced and shifted to lower wavenumber as is the cases of ionic liquids and 1-alkanols, suggesting that the origin of the prepeak of $LiPF_6$/PC solution is similar to that of these liquids. Further works including isotope-substituted scattering experiments and molecular dynamics simulations will be required for the definite assignment.

Given the two characteristic structures in Figure 1, we determined the intermediate scattering functions at the two wavevectors, $q$ = 10 and 14 nm$^{-1}$. The coherent scattering dominates the incoherent one at both wavevectors, keeping in mind that in a NSE measurement the incoherent signal is reduced to 1/3. The intermediate scattering functions obtained with the NSE spectroscopy thus reflect the collective dynamics of solutions.

The normalized intermediate scattering functions at the two wavevectors are shown in Figure 2. The relaxation at both wavevectors becomes slower with increasing the salt concentration, as is expected from the enhanced intermolecular electrostatic interaction and the increased viscosity.

An interesting point to be noted here is the relative relaxation times at the two $q$-values. The relaxation at $q$ = 14 nm$^{-1}$ is slower than that of $q$ = 10 nm$^{-1}$ in neat solvent where the prepeak is absent, which can be understood in terms of de Gennes narrowing. The de Gennes narrowing refers to the slow relaxation of the intermediate scattering function of simple liquids at the main peak of the structure factor, and it is ascribed to the large fluctuation of the density mode.[10] On the other hand, the relaxation at $q$ = 10 nm$^{-1}$ is slower than that at $q$ = 14 nm$^{-1}$ when the lithium salt is dissolved. In the case of the concentration of 1 mol/kg, $I(q,t)/I(q,0)$ at $q$ = 10 nm$^{-1}$ is smaller than that at $q$ = 14 nm$^{-1}$ at $t$ < 20 ps, and the order is inverted at the longer times, which is probably due to the


DOI: 10.1021/acs.jpcb.5b08701
J. Phys. Chem. B 2015, 119, 15675−15682

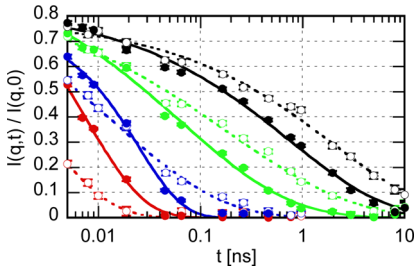


**Figure 2.** Normailzed intermediate scattering functions of $LiPF_6$/PC solutions at 298 K are plotted as a function of Fourier time $t$. The circles with error bars show the experimental values, while the curves do the KWW fitting functions (eq 9). The concentrations are 0 mol/kg (red), 1 mol/kg (blue), 2 mol/kg (green), and 3 mol/kg (black). The filled symbols and solid curves exhibit the intermediate scattering functions at $q$ = 14 $nm^{-1}$, while the open symbols and dotted curves do those at $q$ = 10 $nm^{-1}$. Error bars represent ±1 standard deviation.

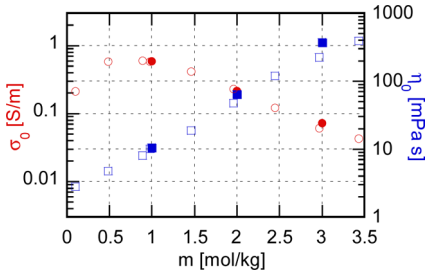


**Figure 3.** DC ionic conductivity (red circles) and the shear viscosity (blue squares) are plotted as a function of the molal concentration $m$. The solid symbols show the values determined in this work, while the open ones do those reported by Kondo and co-workers.[6] The errors in our measurements were described in the Experimental Section.

effects of the edge of the main peak at $q$ = 10 $nm^{-1}$. The slower structural relaxation at the prepeak has been reported on various ionic liquids[12,38] and hydrogen-bonding organic liquids.[13,14] The relaxation of the prepeak is 2−3 times slower than that of the main peak at 3 mol/kg, which is comparable or slightly slower than that of the prediction of the simple diffusion model, $\tau \propto 1/q^2$. Since the relaxation at $q$ = 14 $nm^{-1}$ is affected by the strong structural correlation at the main peak, the similar role of the structural correlation represented as the prepeak is expected for the relaxation at $q$ = 10 $nm^{-1}$. We thus consider that the slower relaxation at $q$ = 10 $nm^{-1}$ is ascribed to the presence of the prepeak.

One may consider that the dynamics of the solution can be described as the superposition of the contributions of the ions and solvents. However, the intermediate scattering function does not exhibit the bimodal relaxation, and the structural relaxation is retarded as a whole with increasing the concentration of the salt. Provided that the molar ratio of the salt and the solvent is 1:3.3 at 3 mol/kg, almost all the solvents are solvated to ions, and the dynamics of both species are strongly coupled.

The next question is how the characteristic prepeak structure and its slow dynamics affect the macroscopic properties of $LiPF_6$/PC solutions such as shear viscosity and ionic conductivity. Hereafter we shall analyze the relationship based on the theory described in section 2. For numerical treatment of the intermediate scattering function, it is now approximated by the Kohlrausch−Williams−Watts (KWW) function as

$$I_n(q, t) = A \exp\left[-\left(\frac{t}{\tau}\right)^{\beta}\right] \quad (9)$$

All the three parameters, $A$, $\tau$, and $\beta$, were treated as the adjustable ones in the fitting procedure. The KWW functions describe $I_n(q,t)$ well, as is demonstrated with the solid and dotted curves in Figure 2. The parameters of the KWW function determined are summarized in Table S1 of the Supporting Information.

**4.2. Frequency-Dependent Transport Properties.** The zero-frequency values of the transport coefficients, $\sigma_0$ and $\eta_0$, are plotted as functions of the salt concentration in Figure 3. The increase in the salt concentration leads to the rapid reduction of the molecular mobility, that is, the decrease in $\sigma_0$ and the increase in $\eta_0$. Compared with the corresponding values reported by Kondo and co-workers,[6] our results agree well with theirs except for the small disagreement in $\eta_0$ at 3 mol/kg.

The normalized shear relaxation spectra at 2 and 3 mol/kg are shown in Figures 4a and 4b, respectively. A large relaxation

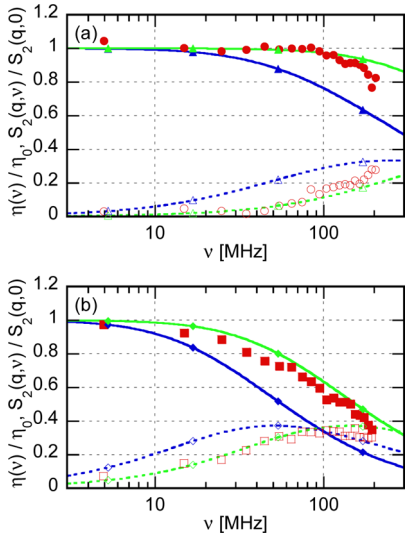


**Figure 4.** Normalized shear relaxation spectra, $\eta(\nu)/\eta_0$ (red), are compared with the normalized relaxation functions calculated from the intermediate scattering functions, $S_2(q,\nu)/S_2(q,0)$ (blue and green for $q$ = 10 and 14 $nm^{-1}$, respectively). The concentrations of the salt are (a) 2 and (b) 3 mol/kg, respectively. The real and imaginary parts are shown with filled and open symbols, respectively. In particular, the solid and dotted lines with filled and open symbols, respectively, show the real and the imaginary parts of $S_2(q,\nu)/S_2(q,0)$. The errors in the shear relaxation spectra are described in the Experimental Section.

is observed in the megahertz region at both concentrations, and the relaxation becomes slower with increasing salt concentration. We have reported similar shear relaxation spectra of $LiClO_4$/PC solutions in our previous work,[7] and the present results on $LiPF_6$/PC show that the presence of the shear relaxation is common to Li-salt solutions in PC irrespective of anions. The result on 1 mol/kg solution is omitted in Figure 4 because no relaxation was found in the frequency window of our experiment, which is also in harmony with our previous work.[7] Since the real part, $\eta'(\nu)$, converges to the steady-state shear viscosity, $\eta_0$, on the low-frequency side, the relaxation shown in Figure 4 represents the dynamics that determine the value of $\eta_0$.



DOI: 10.1021/acs.jpcb.5b08701
J. Phys. Chem. B 2015, 119, 15675−15682

The relaxation functions calculated using the neutron intermediate scattering functions, $S_2(q,\nu)$, are plotted together with the shear relaxation in Figure 4. The spectra at two concentrations and two wavevectors are also shown in the figure. As is expected from the intermediate scattering functions in the time domain (Figure 2), the relaxation frequency decreases with concentration, and the relaxation at the prepeak is slower than that at the main peak. The normalized relaxation function at the main peak approximately agrees with $\eta(\nu)$, while that at the prepeak is much slower than $\eta(\nu)$. The microscopic dynamics that determines $\eta_0$ is therefore ascribed to that at the main peak rather than that at the prepeak.

The relationship between the neutron intermediate scattering function and the shear viscosity has been examined on several systems that possess the prepeak structure. In our previous studies on ionic liquids with long alkyl chains, shear relaxation is as fast as $S_2(q,\nu)$ at the main peak when the shear viscosity is low, and the former becomes increasingly slower than the latter with increasing the viscosity.[11,26] Our present result on $LiPF_6$/PC solutions thus corresponds to the low-viscosity case of ionic liquids. The temperature dependence of the neutron intermediate scattering functions of 1-propanol was studied by Sillrén and co-workers.[14] From the comparison of the temperature dependence of the intermediate scattering functions with that of the shear viscosity, they concluded that the shear viscosity is coupled to the dynamics at the main peak. Given the previous studies above, we consider it is usual for the shear relaxation to be coupled with the structural relaxation at the main peak, even in the presence of a slower relaxation at the prepeak.

Figure 5 shows the AC electric conductivity at all the concentrations. The AC electric conductivity also exhibits a relaxation in the megahertz region, and its relaxation frequency decreases with increasing the salt concentration, as is the case of the shear relaxation. The concentration dependence of the AC conductivity spectra is similar to those of $LiClO_4$/PC solutions in our previous study.[7] However, the relaxation frequency of the AC conductivity is lower than that of the shear relaxation in Figure 4. Since the former relaxation is comparable to or faster than the latter one in the case of ionic liquids,[39,40] the relationship between the frequency dependences of the electric conductivity and the shear viscosity of the concentrated electrolyte solution is different from those of ionic liquids.

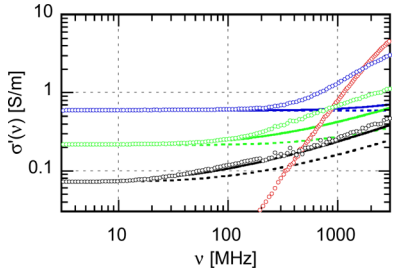


**Figure 5.** Real parts of the AC conductivity of $LiPF_6$/PC solutions are plotted as a function of the frequency $\nu$ with open circles. The concentrations are 0 mol/kg (red), 1 mol/kg (blue), 2 mol/kg (green), and 3 mol/kg (black). The spectrum of the neat solvent was taken from ref 7. The corresponding functions calculated from the neutron intermediate scattering functions, $\mathrm{Re}[\sigma_0 + S_2(q,0)/S_2(q,\nu)]$, are also shown for comparison. The values of $q$ are 10 and 14 $nm^{-1}$ for solid and dotted curves, respectively.

The important difference between the electrolyte solutions and the ionic liquids is, however, that there are polar solvents in the former, which also contribute to the apparent AC conductivity through the reorentational relaxation. Figure 5 includes a plot for the AC electric conductivity of the neat solvent; the data are taken from ref 7. Since the value of $\sigma'(\nu)$ of neat solvent is larger than those of electrolyte solutions, the contribution of the reorientational relaxation of the solvent to $\sigma'(\nu)$ can be neglected by no means. On the other hand, $\sigma'(\nu)$ of ionic liquids can be assigned wholly to the motion of ions. Although the reorientational relaxation of ions may also contribute to $\sigma'(\nu)$ in principle, our theoretical and experimental studies suggested that its contribution is rather minor.[41−43]

The AC conductivity is compared with the reciprocal relaxation functions at the two wavevectors in Figure 5. The relaxation of $\sigma'(\nu)$ is slower than those of $S_2(q,\nu)$ at both wavevectors at 1 and 2 mol/kg, which is mainly ascribed to the contribution of the solvent. The difference between $\sigma'(\nu)$ and $1/S_2(q,\nu)$ decreases with increasing the salt concentration because the contribution of the solvent decreases with concentration due to the decreased number density of the solvent. At 3 mol/kg, surprisingly enough, the AC conductivity agrees with the relaxation function calculated from the intermediate scattering function at the prepeak. If the AC electric conductivity at 3 mol/kg is dominated by the ionic contribution, $\sigma_I(\nu)$, the agreement between $\sigma_I(\nu)$ and $1/S_2(q,\nu)$ at the prepeak means that the ionic conduction is coupled with the dynamics of the intermediate-range structure represented by the prepeak.

We cannot of course exclude the possible contribution of the reorientational relaxation of the solvent to the AC electric conductivity at 3 mol/kg. It is possible that the agreement between $\sigma_I(\nu)$ and $1/S_2(q,\nu)$ at the prepeak is a mere coincidence and that the former is explained by the superposition of the structural relaxation at the main peak and the reorientational relaxation of the solvent. It is impossible to separate the solvent and ionic components solely on experimental bases. Although the division into two terms can be performed by fitting procedures using model functions, the results depend strongly on the choice of the model functions. Some kinds of computational studies, such as molecular dynamics simulations or the MCT calculations, will be required for the extraction of the AC ionic conductivity.

We have three plans at present for our future work on the concentrated organic electrolytes. The first one is on the assignment of the prepeak, for which computational and theoretical methods will be powerful tools. On experimental sides, the isotope substituted neutron diffraction is available. It will be also interesting to study on a series of electrolytes changing the cation, anion, and solvent separately. Preliminary results of such experiments are already exhibited in Figure S1 of the Supporting Information. The second plan is computational studies on dynamics. The extraction of $\sigma_I(\nu)$ from $\sigma(\nu)$ as was described in the previous paragraph is of course one of the aims there. In addition, the origin of the slow structural relaxation shall be analyzed. The third one is the temperature dependence of the structural relaxation time and the transport coefficients. Computational and theoretical studies on model supercooled liquids demonstrate that the relaxation of the shear stress becomes slower than that of the intermediate scattering function at the main peak on supercooling, and the decoupling between the shear stress and the structural relaxation is the


DOI: 10.1021/acs.jpcb.5b08701
J. Phys. Chem. B 2015, 119, 15675−15682

reason for the violation of the Stokes−Einstein relationship between the shear viscosity and the self-diffusion coefficient.[44,45] We have found a similar trend in a series of ionic liquids in our previous work.[21,39] In the present case on the organic electrolyte, however, the decoupling is scarcely observed with increasing the salt concentration, and the temperature dependence on the dynamics of the present system shall be analyzed in order to examine whether the structure−stress decoupling is a universal behavior of viscous liquids that holds also on concentrated organic electrolytes.

## 5. CONCLUSION

The structural relaxation dynamics of concentrated $LiPF_6$/PC solutions was investigated with NSE spectroscopy, and the obtained relaxation functions were compared with the shear relaxation spectra and AC conductivity in order to clarify the relationship between the liquid structure and the transport coefficients.

The static neutron diffraction of the concentrated solution exhibited the prepeak at 10 $nm^{-1}$ in addition to the main peak at 14 $nm^{-1}$ that is common to neat solvent, which indicates a intermediate-range structure in the concentrated organic electrolytes. The relaxation of the intermediate scattering function at the prepeak was several times slower than that at the main peak.

The shear relaxation spectra of concentrated solutions agree with those calculated from the structural relaxation at the main peak based on MCT, which means that the liquid structure represented as the main peak is responsible for the shear viscosity. On the other hand, the relaxation of the prepeak matches with the AC conductivity at the highest concentration studied in this work, 3 mol/kg, suggesting a possible contribution of the intermediate structure to the ionic conduction. However, the separation of the ionic and solvent contributions to the AC conductivity is required in order to achieve the definitive conclusion.

## ■ ASSOCIATED CONTENT

### Supporting Information

The Supporting Information is available free of charge on the ACS Publications website at DOI: 10.1021/acs.jpcb.5b08701.

X-ray and neutron diffraction patterns of the solution of $LiPF_6$ in alkylene carbonates and the KWW parameters of the fitting curves in Figure 2 (PDF)

## ■ AUTHOR INFORMATION

### Corresponding Author

*E-mail tyama@nuce.nagoya-u.ac.jp, Tel +81-52-789-3592, Fax +81-52-789-3273 (T.Y.).

### Notes

The authors declare no competing financial interest.

## ■ ACKNOWLEDGMENTS

Tsuyoshi Yamaguchi and Takuya Yonezawa are grateful to Prof. Shinobu Koda (Nagoya Univ.) for the use of facilities in his laboratory and fruitful discussions. We thank Leland Harriger (NCNR, NIST) for his support of our diffraction measurements on SPINS. This work is partly supported by the Japan Society for the Promotion of Science (JSPS), KAKENHI grant 24550019. Michihiro Nagao acknowledges funding support of cooperative agreement 70NANB10H255 from NIST, U.S. Department of Commerce. This work utilized facilities supported in part by the National Science Foundation under agreement DMR-0944772. Travel expenses of Tsuyoshi Yamaguchi and Koji Yoshida for the NSE experiment performed using NGA-NSE at NCNR, NIST, USA, were supported by General User Program for Neutron Scattering Experiments, Institute for Solid State Physics, The University of Tokyo (proposal no. 14601), at JRR-3, Japan Atomic Energy Agency, Tokai, Japan.

## ■ REFERENCES

(1) Hayamizu, K.; Aihara, Y.; Arai, S.; Martinez, C. G. Pulse-Gradient Spin-Echo $^1H$, $^7Li$, and $^{19}F$ NMR Diffusion and Ionic Conductivity Measurements of 14 Organic Electrolytes Containing $LiN(SO_2CF_3)_2$. *J. Phys. Chem. B* **1999**, *103*, 519−524.

(2) Aihara, Y.; Sugimoto, K.; Price, W. S.; Hayamizu, K. Ionic Conduction and Self-Diffusion Near Infinitesimal Concentration in Lithium Salt-Organic Solvent Electrolytes. *J. Chem. Phys.* **2000**, *113*, 1981−1991.

(3) Yoshida, K.; Nakamura, M.; Kazue, Y.; Tachikawa, N.; Tsuzuki, S.; Seki, S.; Dokko, K.; Watanabe, M. Oxidative-Stability Enhancement and Charge Transport Mechanism in Glyme-Lithium Salt Equimolar Complexes. *J. Am. Chem. Soc.* **2011**, *133*, 13121−13129.

(4) Yamada, Y.; Furukawa, K.; Sodeyama, K.; Kikuchi, K.; Yaegashi, M.; Tateyama, Y.; Yamada, A. Unusual Stability of Acetonitrile-Based Superconcentrated Electrolytes for Fast-Charging Lithium-Ion Batteries. *J. Am. Chem. Soc.* **2014**, *136*, 5039−5046.

(5) Southall, J. P.; Hubbard, H. V.; St, A.; Rogers, J. V.; Davies, G. R.; McIntyre, J. E.; Ward, I. M. Ionic Conductivity and Viscosity Correlations in Liquid Electrolytes for Incorporation into PVDF Gel Electrolytes. *Solid State Ionics* **1996**, *85*, 51−60.

(6) Kondo, K.; Sano, M.; Hiwara, A.; Omi, T.; Fujita, M.; Kuwae, A.; Iida, M.; Mogi, K.; Yokoyama, H. Conductivity and Solvation of $Li^+$ Ions of $LiPF_6$ in Propylene Carbonate Solutions. *J. Phys. Chem. B* **2000**, *104*, 5040−5044.

(7) Yamaguchi, T.; Hayakawa, M.; Matsuoka, T.; Koda, S. Electric and Mechanical Relaxations of $LiClO_4$-Propylene Carbonate Systems in 100 MHz Region. *J. Phys. Chem. B* **2009**, *113*, 11988−11998.

(8) *Theory of Simple Liquids*, 2nd ed.; Hansen, J.-P., McDonald, I. R., Eds.; Academic Press: London, 1986.

(9) *Molecular Hydrodynamics*; Boon, J.-P., Yip, S., Eds.; Dover Publications: New York, 1991.

(10) *Dynamics of the Liquid State*; Balucani, U., Zoppi, M., Eds.; Clarendon Press: Oxford, 1994.

(11) Yamaguchi, T.; Mikawa, K.; Koda, S.; Fujii, K.; Endo, H.; Shibayama, M.; Hamano, H.; Umebayashi, Y. Relationship between Mesoscale Dynamics and Shear Relaxation of Ionic Liquids with Long Alkyl Chain. *J. Chem. Phys.* **2012**, *137*, 104511.

(12) Yamamuro, O.; Yamada, T.; Kofu, M.; Nakakoshi, M.; Nagao, M. Hierarchical Structure and Dynamics of an Ionic Liquid 1-Octyl-3-methylimidazolium Chloride. *J. Chem. Phys.* **2011**, *135*, 054508.

(13) Faraone, A.; Hong, K.; Kneller, L. R.; Ohl, M.; Copley, J. R. D. Coherent Dynamics of Meta-Toluidine Investigated by Quasielastic Neutron Scattering. *J. Chem. Phys.* **2012**, *136*, 104502.

(14) Sillrén, P.; Matic, A.; Karlsson, M.; Koza, M.; Maccarini, M.; Fouquet, P.; Götz, M.; Bauer, Th.; Gulich, R.; Lunkenheimer, P.; et al. Liquid 1-Propanol Studied by Neutron Scattering, Near-Infrared, and Dielectric Spectroscopy. *J. Chem. Phys.* **2014**, *140*, 124501.

(15) Prevel, B.; Dupuy-Philon, J.; Jal, J. F.; Legrand, J. F.; Chieux, P. Structural Relaxation in Supercooled Glass-Forming Solutions: a Neutron Spin-Echo Study of LiCl, $6D_2O$. *J. Phys.: Condens. Matter* **1994**, *6*, 1279−1290.

(16) Kanaya, T.; Inoue, R.; Saito, M.; Seto, M.; Yoda, Y. Relaxation Transition in Glass-Forming Polybutadiene as Revealed by Nuclear Resonance X-Ray Scattering. *J. Chem. Phys.* **2014**, *140*, 144906.

(17) Mei, Q.; Benmore, C. J.; Sen, S.; Sharma, R.; Yarger, J. L. Intermediate Range Order in Vitreous Silica from a Partial Structure Factor Analysis. *Phys. Rev. B: Condens. Matter Mater. Phys.* **2008**, *78*, 144204.



DOI: 10.1021/acs.jpcb.5b08701
*J. Phys. Chem. B* 2015, 119, 15675−15682

(18) Morineau, D.; Alba-Simionesco, C. Hydrogen-bond-induced Clustering in the Fragile Glass-Forming Liquid m-Toluidine: Experiments and Simulation. *J. Chem. Phys.* **1998**, *109*, 8494−8503.
(19) Tomšič, M.; Bešter-Rogač, M.; Jamnik, A.; Kunz, W.; Touraud, D.; Bergmann, A.; Glatter, O. Nonionic Surfactant Brij 35 in Water and in Various Simple Alcohols: Structural Investigations by Small-Angle X-Ray Scattering and Dynamic Light Scattering. *J. Phys. Chem. B* **2004**, *108*, 7021−7032.
(20) Tomšič, M.; Jamnik, A.; Fritz-Popovski, G.; Glatter, O.; Vlček, L. Structural Properties of Pure Simple Alcohols from Ethanol, Propanol, Butanol, Pentanol, to Hexanol: Comparing Monte-Carlo Simulations with Experimental SAXS Data. *J. Phys. Chem. B* **2007**, *111*, 1738−1751.
(21) Canongia Lopes, J. N. A.; Pádua, A. A. H. Nanostructural Organization in Ionic Liquids. *J. Phys. Chem. B* **2006**, *110*, 3330−3335.
(22) Russina, O.; Triolo, A. New Experimental Evidence Supporting the Mesoscopic Segregation Model in Room Temperature Ionic Liquids. *Faraday Discuss.* **2012**, *154*, 97−109.
(23) Fujii, K.; Kanzaki, R.; Takamuku, T.; Kameda, Y.; Kohara, S.; Kanakubo, M.; Shibayama, M.; Ishiguro, S.; Umebayashi, Y. Experimental Evidences for Molecular Origin of Low-Q Peak in Neutron/X-Ray Scattering of 1-Alkyl-3-methylimidazolium Bis-(trifluoromethanesulfonyl)amide Ionic Liquids. *J. Chem. Phys.* **2011**, *135*, 244502.
(24) Shimizu, K.; Bernardes, C. E. S.; Canongia Lopes, J. N. Structure and Aggregation in the 1-Alkyl-3-Methylimidazolium Bis-(trifluoromethylsulfonyl)imide Ionic Liquid Homologous Series. *J. Phys. Chem. B* **2014**, *118*, 567−576.
(25) Rocha, M. A. A.; Neves, C. M. S. S.; Freire, M. G.; Russina, O.; Triolo, A.; Coutinho, J. A. P.; Santos, L. M. N. B. F. Alkylimidazolium Based Ionic Liquids: Impact of Cation Symmetry on Their Nanoscale Structural Organization. *J. Phys. Chem. B* **2013**, *117*, 10889−10897.
(26) Yamaguchi, T.; Yonezawa, T.; Koda, S. Study on the Temperature-dependent Coupling Among Viscosity, Conductivity and Structural Relaxation of Ionic Liquids. *Phys. Chem. Chem. Phys.* **2015**, *17*, 19126−19133.
(27) Chong, S.-H.; Götze, W. Idealized Glass Transitions for a System of Dumbbell Molecules. *Phys. Rev. E: Stat. Phys., Plasmas, Fluids, Relat. Interdiscip. Top.* **2002**, *65*, 041503.
(28) Rosov, N.; Rathgeber, S.; Monkenbusch, M. Neutron Spin Echo spectroscopy at the NIST Center for Neutron Research. *ACS Symp. Ser.* **2000**, *739*, 103−116.
(29) Azuah, R. T.; Kneller, L. R.; Qiu, Y.; Tregenna-Piggott, P. L. W.; Brown, C. M.; Copley, J. R. D.; Dimeo, R. M. DAVE: A Comprehensive Software Suite for the Reduction, Visualization, and Analysis of Low Energy Neutron Spectroscopic Data. *J. Res. Natl. Inst. Stand. Technol.* **2009**, *114*, 341−358.
(30) Behrends, R.; Kaatze, U. A High Frequency Shear Wave Impedance Spectrometer for Low Viscosity Liquids. *Meas. Sci. Technol.* **2001**, *12*, 519−524.
(31) Yamaguchi, T.; Mikawa, K.; Koda, S. Shear Relaxation of Water-ionic Liquid Mixtures. *Bull. Chem. Soc. Jpn.* **2012**, *85*, 701−705.
(32) Yamaguchi, T.; Yamada, Y.; Koda, S. Shear and Conductivity Relaxations of Lithium Ion Electrolytes in Polyethyleneglycol Eimethyl Ethers. *J. Mol. Liq.* **2012**, *172*, 93−101.
(33) Buchner, R.; Hefter, G. T.; May, P. M. Dielectric Relaxation of Aqueous NaCl Solutions. *J. Phys. Chem. A* **1999**, *103*, 1−9.
(34) Aguilera, L.; Xiong, S.; Scheers, J.; Matic, A. A Structural Study of LiTFSI-tetraglyme Mixtures: From Diluted Solutions to Solvated Ionic Liquids. *J. Mol. Liq.* **2015**, *210*, 243−251.
(35) Shimizu, K.; Freitas, A. A.; Atkin, R.; Warr, G. G.; FitzGerald, P. A.; Doi, H.; Saito, S.; Ueno, K.; Umebayashi, Y.; Watanabe, M.; et al. Structural and Aggregate Analyses of (Li Salt + Glyme) Mixtures; the Complex Nature of Solvate Ionic Liquids. *Phys. Chem. Chem. Phys.* **2015**, *17*, 22321−22335.
(36) Seo, D. M.; Afroz, T.; Allen, J. L.; Boyle, P. D.; Trulove, P. C.; De Long, H. C.; Henderson, W. A. Structural Interactions within Lithium Salt Solvates: Cyclic Carbonates and Esters. *J. Phys. Chem. C* **2014**, *118*, 25884−25889.
(37) Kashyap, H. K.; Hettige, J. J.; Annapureddy, H. V. R.; Margulis, C. J. SAXS Anti-Peaks Reveal the Length-Scales of Dual Positive−Negative and Polar−Apolar Ordering in Room-Temperature Ionic Liquids. *Chem. Commun.* **2012**, *48*, 5103−5105.
(38) Kofu, M.; Nagao, M.; Ueki, T.; Kitazawa, Y.; Nakamura, Y.; Sawamura, S.; Watanabe, M.; Yamamuro, O. Heterogeneous Slow Dynamics of Imidazolium-Based Ionic Liquids Studied by Neutron Spin Echo. *J. Phys. Chem. B* **2013**, *117*, 2773−2781.
(39) Šantić, A.; Wrobel, W.; Mutke, M.; Banhatti, R.; Funke, K. Frequency-dependent Fluidity and Conductivity of an Ionic Liquid. *Phys. Chem. Chem. Phys.* **2009**, *11*, 5930−5934.
(40) Yamaguchi, T.; Nakahara, E.; Koda, S. Quantitative Analysis of Conductivity and Viscosity of Ionic Liquids in Terms of Their Relaxation Times. *J. Phys. Chem. B* **2014**, *118*, 5752−5759.
(41) Yamaguchi, T.; Koda, S. Mode-coupling Theoretical Analysis of Transport and Relaxation Properties of Liquid Dimethylimidazolium Chloride. *J. Chem. Phys.* **2010**, *132*, 114502.
(42) Yamaguchi, T.; Koda, S. Assignment of the Dielectric Relaxation of Ionic Liquid and its Implication to the Ionic Conduction Mechanism. *J. Mol. Liq.* **2011**, *164*, 49−52.
(43) Yamaguchi, T.; Koda, S. Dielectric and Shear Relaxations of Ionic Liquid Composed of Symmetric Ions. *J. Chem. Phys.* **2014**, *141*, 144503.
(44) Zangi, R.; Kaufman, L. J. Frequency-Dependent Stokes-Einstein Relation in Supercooled Liquids. *Phys. Rev. E* **2007**, *75*, 051501.
(45) Kim, K.; Saito, S. Role of the Lifetime of Dynamic Heterogeneity in the Frequency-Dependent Stokes-Einstein Relation of Supercooled Liquids. *J. Phys. Soc. Jpn.* **2010**, *79*, 093601.
(46) Certain trade names and company products are identified in order to specify adequately the experimental procedure. In no case does such identification imply our recommendation or endorsement, nor does it imply that the products are necessarily the best for the purpose.


DOI: 10.1021/acs.jpcb.5b08701
*J. Phys. Chem. B* 2015, 119, 15675−15682